Engineering Geology 168 (2014) 59–68

Contents lists available at ScienceDirect

Engineering Geology

journal homepage: www.elsevier.com/locate/enggeo

Integrated seismic and cone penetration test observations at a distressed earthen levee: Marrero, Louisiana, U.S.A.

Juan M. Lorenzo [a,*], Jason Hicks [b], Emilio E. Vera [b]

[a] Department of Geology and Geophysics, Louisiana State University, Baton Rouge, LA 70803-4101, USA
[b] Departamento de Geofísica, Facultad de Ciencias Físicas y Matemáticas, Blanco Encalada 2002, Universidad de Chile, Santiago, Chile

ARTICLE INFO

Article history:
Received 23 March 2012
Received in revised form 17 October 2013
Accepted 22 October 2013
Available online 29 October 2013

Keywords:
Near-surface
Levees
Reflection
Geophysics
Seismology
Geotechnical

ABSTRACT

Seismic refraction velocity-versus depth models can complement our understanding of natural soils beneath flood protection levees at locations between geotechnical sites. Levee failures in New Orleans in 2005 are attributable in part to poor understanding of sediments between geotechnical sites. To a first order, subsurface fluvial–deltaic facies in the lower Mississippi delta plain correlate with general geotechnical properties of water content and cohesive strength, but are too laterally variable to be easily predicted from geotechnical sites spaced 100 m apart. An artificial earthen levee, suitable for seismic investigation, lies ~15 km S of the city of New Orleans, Louisiana. Values of shear-wave velocity (V_{SH}) versus depth (0–20 m) are derived by forward-ray-trace models of seismic refraction arrivals which match key boundaries identified at (geotechnical) cone-penetration testing sites, spaced at 300 m apart. In particular, a 100-m section along the levee crest shows continuous cracks which are as much as 10 cm wide, and 30 cm deep at their northern end. Cracking may relate to high strain, induced by variable near-surface subsidence of organic-rich sediments. Topographic cross-sections across the levee show variable differential subsidence of 1–2 m. Based on effective medium theory, V_P- and V_{SH}-versus-depth profiles indicate unexpectedly greater saturation and lower shear moduli on the unprotected levee side adjacent to the cracks.

Integration of geophysical, sedimentary and topographic data, even if only at a few locations can help locate anomalous zones in sub-levee soil between geotechnical boring sites. Future preventive monitoring of flood-protection barriers stands to benefit greatly from integrated data sets "ground truthed" to geotechnical data.

1. Introduction

Despite an understanding of the processes leading to levee failures, insufficient characterization of natural sub-levee soil conditions continues to influence levee construction and impact their longer-term integrity. Evenly spaced geotechnical sampling provides precise measurements of properties (e.g., soil behavior types, water content) but only at specific sites. For example, cone penetration testing (CPT) is a common geotechnical practice (e.g., Fellenius and Eslami, 2000) used to infer soil behavior types from the stress at the head of the tip of the tool (q_c) and friction along its sides (f_s) as it is pushed through soil at a constant rate. However, Rogers et al.'s (2008) analysis of multiple levee failures in New Orleans in 2005, after hurricane Katrina, shows that linear interpolation of geotechnical properties between existing borehole data over distances of ~600 m are insufficient to characterize the diverse/laterally variable set of sedimentary units present in this lower delta (Figure 1). Independent studies by experts suggest that maintenance and monitoring of these structures require a novel approach (Andersen et al., 2007).

For levee evaluation and long-term monitoring, continuous seismic profiles can be used to fill the gaps in subsurface geotechnical properties between borehole sites. Seismic profiles have the potential to highlight anomalous zones and direct more localized geotechnical sampling in a more focus efficient manner (Niederleithinger et al., 2012). Seismic properties (e.g., shear (V_S) and compressional-wave (V_P) velocities) can be correlated at borehole tie-points; to meaningful geotechnical properties (Na et al., 2005), such as soil behavior types which are associated with equivalent grain size behaviors (Robertson, 1990) and engineering shear strength estimates (Lane et al., 2008). Shear-wave velocity within the levee fill can be derived from the analysis of surface-waves along the levee center (Dunbar et al., 2007) or from more traditional refracted S_H waves. Although more sophisticated well-known geostatistical methods exist that better take into account the lateral heterogeneity of soil properties (e.g., kriging) these remain underused in the geotechnical field (Hammah and Curran, 2006).

Ground truthing is essential to maintain the accuracy of borehole-to-seismic correlations in a levee system. In some cases seismic anomalies may correspond to normal construction conditions. Fill within an artificial levee is usually locally derived, and can be made heterogeneous through the process of repeated building episodes. Inherent uncertainties in the engineering analyses (Seed et al., 2006) and

* Corresponding author. Tel.: +1 225 578 4249; fax: +1 225 578 2302.
E-mail address: gllore@lsu.edu (J.M. Lorenzo).

0013-7952/$ – see front matter © 2013 Elsevier B.V. All rights reserved.
http://dx.doi.org/10.1016/j.enggeo.2013.10.019

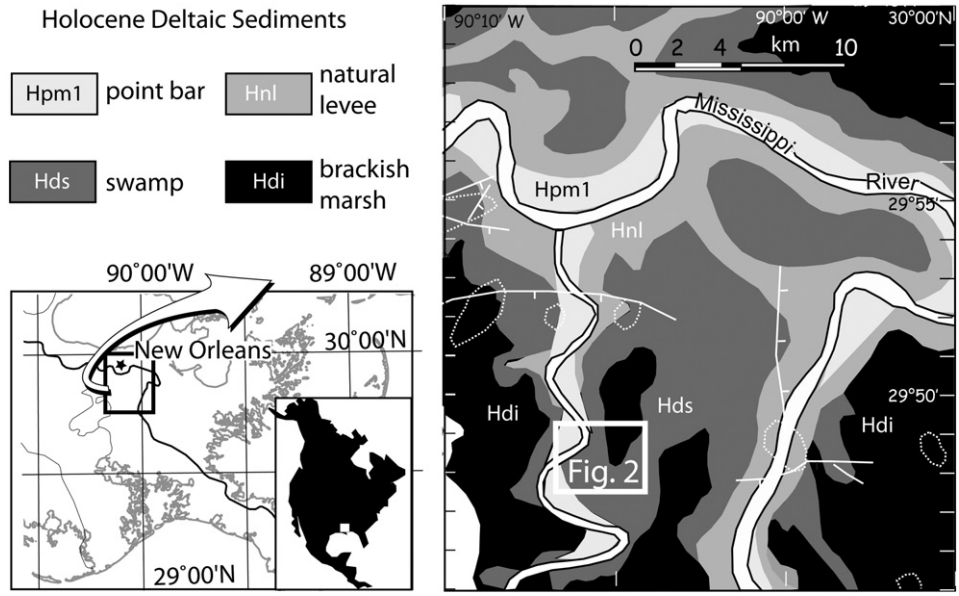

Fig. 1. Regional location and sedimentary setting. Study area (white box) along northern Gulf of Mexico Coast, USA, lies south of the city of New Orleans (left insets). Mapped surface sedimentary facies (Saucier, 1994) are expected to represent near-surface (0–20 m) sediments. Traces of buried faults (thin white lines hachured in the direction of fault block drop) (Wallace, 1957) and salt domes (dashed white lines) surround but do not cross study area.

unexpected variability in the foundation soils can be checked independently through these geophysical methods. Correlations at common locations between low-strain seismic shear modulus and geotechnical data (e.g., Hegazy and Mayne, 1995) should be conducted as regularly as possible.

Near-surface (0–20 m) hydrogeologic processes in the natural soils beneath artificial levees (levees, dikes) may contribute to their structural failure. Specifically, differential rates of compaction within the natural soil or embankment fill (Akpokodje, 1989) can help create zones of high strain or local cracking. Floodplain and lower delta deposits rich in highly porous, organic-rich soils are most susceptible to natural compaction (Nyman et al., 1990) especially in the protected areas behind levees. Exposure to additional oxygen accelerates decomposition (Galloway et al., 1999) and can lower the protected land surface no longer replenished by new sediments from the unprotected side of the levees, at rates of 10^{-3}–10^{-2} m/yr (Turner, 2004). Organic soils tend to confer lower shear strength (e.g., Ulusay et al., 2010) so shear failure of slopes is not uncommon in floodplains (Mesri and Ajlouni, 2007) such as the Sacramento-San Joaquin delta area where over 100 levee failures have taken place since the early 1890s (Galloway et al., 1999). As well, below the surface, shallow seepage through cracked soils may also facilitate failure though eventual slip and erosion (Dyer, 2005). Deep seepage between the protected side and flood side of the embankment can build up excessive hydrostatic pressure thus facilitating slip above relatively impervious layers (Julien, 2002), or even initiate fluid flow leading to blowouts (Cobos-Roa and Bea, 2008) and sand boils (Dunbar et al., 1999).

Purely hydrological mechanisms can also induce bank failure of the engineered fill that overlies natural sub-levee soils. Levee undercutting (Dunbar et al., 1999) occurs naturally on the outer bends of river meanders where the cross-sectional stream velocity is fastest (Turnbull et al., 1966; Gagliano and van Beek, 1970; Reading, 1998; Miall, 2000). Overtopping, accompanied by sufficient erosion of bank soils (Lee et al., 2009), especially those weakened by poor compaction, may also lead to breaching (Link and Jaeger, 2009).

Herein we examine near-surface (0–20 m) seismic data collected between known geotechnical boring sites, and compare derived seismic velocities against interpreted (from cone-penetrating testing) soil behavior types, collected along a lower delta floodplain levee (artificial) in the Greater New Orleans (U.S.A.) area. Unexpected cracks along the levee crest exist which provide an opportunity to investigate possible causes of the distress.

Based on previous work on New Orleans levees (Lane et al., 2008), seismic data collection along the levee crest is susceptible to the effects of the levee geometry. Along the crest, seismic wavelengths (10's of meters or less) can be comparable to the width of the levee bodies which can act as flexural waveguides and superimpose dispersive wave noise on conventional Rayleigh wave arrivals (Miller and Ivanov, 2005; Karl et al., 2011). As well, if the levee fill is overall weaker than the underlying natural foundation, high-velocity refractions and mode conversions between compressional (P) and shear (S_H) waves can make arrival identification in seismic records more difficult. Seismic data acquisition on the flatter levee flanks, where the fill is normally thinner, should improve data quality and allow for simpler seismic interpretations. In order to minimize interpretational ambiguities in near-surface levee studies (Inazaki and Tadahiko, 2005), we employ multiple geophysical and geotechnical data types, including historical maps, geomorphic facies maps, detailed land and airborne topography (Figure 2), and body-wave seismic data.

While electromagnetic methods have been in common use for many years (e.g. Zhody et al., 1974; Neill, 1990) and are considered essential in groundwater investigations (Santamarina et al., 2005), in their absence, concomitant changes in V_P and V_S values can be used as indicators of proximity to the water table (e.g., Grelle and Guadagno, 2009). In semi-arid fluvial sediments, especially after prolonged drought conditions, V_P–V_S ratios have also been used to highlight anomalously weak areas (Dunbar et al., 2007). Although in the New Orleans area, rainfall is high (>1600 mm/yr; NOAA, 2011), and sub-levee soils lie below sea-level, under these conditions, anomalous V_P/V_S values can still indicate under-compacted materials and/or organic-rich sediments, both of which are structurally weak and prone to failure (Rogers et al., 2008).

2. Geological and geotechnical setting of study area

A suitable levee system for evaluation of the seismic method lies ~15 km south of the city of New Orleans, Louisiana (Figure 1), within an area that contains geotechnical boring sites (Figure 2). We chose to investigate a segment ~1000 m long that follows the eastern branch of a V-shaped historical property boundary (U.S. Geol. Surv., 1947)

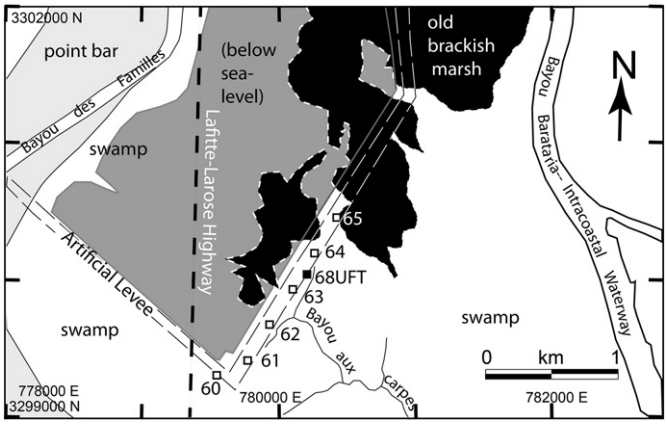

Fig. 2. Study area. Seismic and geotechnical data shown in this paper were collected along the south-eastern side of "V-shaped" artificial levee (dashed lines). We use data from seven (7) geotechnical wells (numbered boxes) that include cone penetrometer testing (solid-white) and laboratory physical properties (solid-black box; Figure 4; FFEB, 2007). Based on LiDAR elevation data (USACE, 2003), the point bar deposits (lighter gray areas; also in Figure 1) lie above sea-level. The darker-shaded area between the point bar and protected by the levee lies below sea-level. (A narrow, water-filled borrow pit lies between the low-land area and the levee.) Aerial photo interpretations (U. S. Navy, 1952) confirm that existence of brackish/fresh water marsh areas and wooded regions over swamp/point bar/natural levee deposits.

(Figure 2). Along this segment, the subsurface soil structure appears simpler than to the north, an area built over an infilled oil-field canal (pers. com., Spohrer, 2008). However, since its original construction in 1991, crest-parallel surface cracks have appeared within our study area (Figures 2, 3). These cracks persist despite the fact that the artificial levee was upgraded three times in subsequent years (pers. com., Merritt, 2007). Along the levee top we trace a ~100 m-long, continuous crack (GPS +/− 1 m) that is relatively straight to the south but which became curvilinear to the north (Figure 3). The crack is most noticeable at the northern end where it is as wide as 10 cm and up to 30 cm deep and where the greatest vertical surface displacement across the crack is ~10 cm down toward the flood-protected side (W). The curvilinear crack near the levee crest is a common precursor to slope failure in the case of a cohesive soil such as clay (Bromhead, 1986).

Near-surface sedimentary facies (Figures 1, 2) (Kolb and Van Lopik, 1958; Saucier, 1994; Dunbar and Britsch, 2008) most likely share geotechnical characteristics with the upper 20 m of Holocene sediments (Figure 4). Vegetative distribution, pre-dating levee construction and noted in aerial photographs (U. S. Navy, 1952), corresponds well to the mapped surface sedimentary facies (Figure 2).

Since ~7 kyr bp, when rates of global sea level rise decelerated (Tornqvist et al., 2004; Peltier and Fairbanks, 2006), 6 major progradational delta lobes built the coastline seaward (Frazier, 1967). In our project area, the most recent Plaquemines–Balize lobe (1.3–0 kyr) is responsible for the first ~4–5 m of sediment consisting of swamp and marsh deposits. Immediately below this, lies the reworked sand-rich top of the St. Bernard Delta Lobe, active in the Holocene between ~4 ky and 2 ky bp (McFarlan, 1961; Frazier, 1967), and underlain by prodelta clays.

In the Mississippi lower delta area, we anticipate that organic-rich marsh deposits will be mechanically weak (Kolb and Van Lopik, 1958; Saucier, 1994) with a high water content (>60%) as found in other deltas globally (Wehling et al., 2003, San Joaquin delta; Akpokodje, 1989, Niger delta). Freshwater marsh soils can have >80% of their volume constituted by water and gases including hydrogen sulfide (Nyman et al., 1990). Formation of weak, under-consolidated, delta soils (Boutwell, 2007) is assisted by high sedimentation rates, 60–100 m over the last 18 ky bp (Blum and Roberts, 2009), and a relatively slow dewatering history.

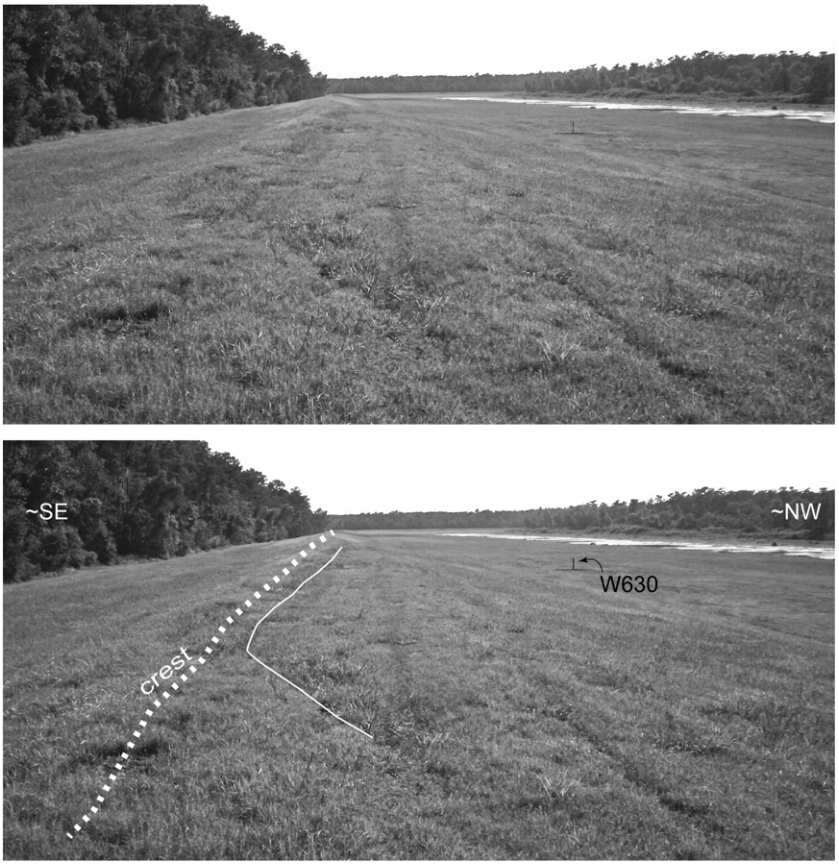

Fig. 3. Levee cracks. Views along "V-line" levee, looking south, display surface cracks along the crest (top, uninterpreted). Water-filled borrow pit lies NW of levee. Point W630 indicates survey marker.

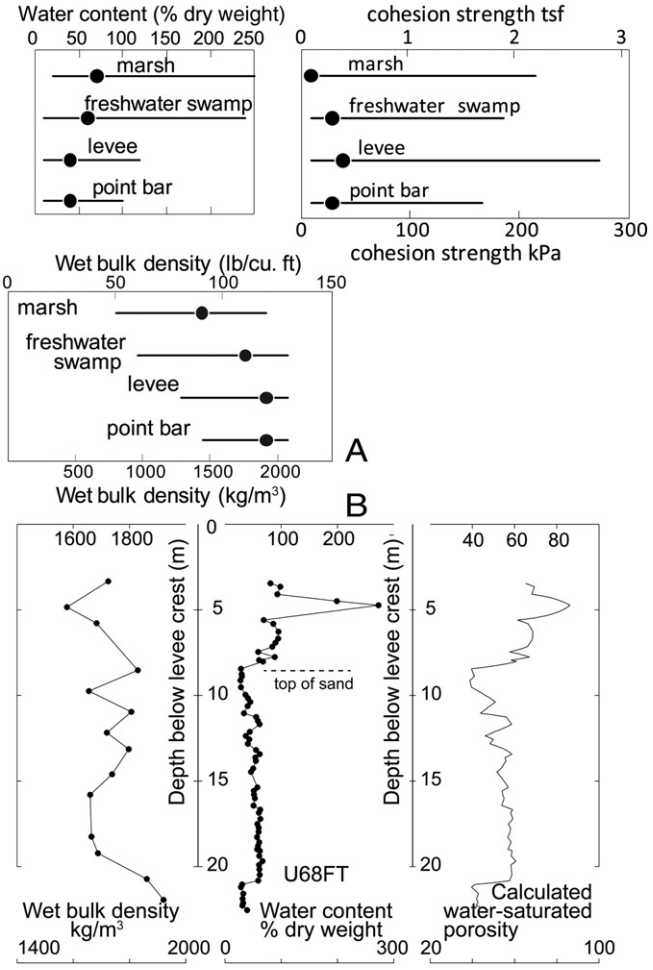

Fig. 4. Physical properties: (A) Relate percent water content (ratio of water content to dry weight), wet bulk density and cohesive strength to dominant lower-delta sedimentary facies (adapted from Saucier, 1994). Large dot marks mode in data distribution. (B) Well 68UFT data (Figures 2, 5, 11; FFEB, 2007) is referenced to the top of a sand-rich unit interpreted for CPT data (Figure 11). Water-saturated porosity is calculated assuming a grain density of 2300 kg/m^3.

Table 1
Equipment, their accuracy, and seismic algorithms used to collect and display the seismic data.

Seismic acquisition	
Geophone separation	1 m
source–receiver offset	1–168 m (site A′), 1–72 m others
Geophones	Mark Products L-28D 30 Hz 410 Ohm coil for horizontal- and OYO GS-100Hz, 600 Ω, for vertical-component sensors.
Seismograph	24-Channel, 24-bit resolution, R24 Geometrics Strataview.
Sample rate, record length	2000 S/s, 2 s.
Seismic sources:	For vertical blows: ~15.25 cm × ~15.25 cm × ~2.5 (6 × 6 × 1 in.) aluminum plate; using ~4.5 kg (10-lb) sledge hammer. For horizontal blows: ~8.4 kg (9-lb) sledge-hammer; Small I beam ~3.2 mm (1/8 ″-steel), kg each head of the "I" is ~15.25 cm (6″) wide by ~28 cm (11″) long and separated by 16.5 cm (6.5″); using ~4.5 kg (10-lb) sledge hammer.
Radio-controlled start of recording	Ario Labs seismic radio-trigger 423 MHz.
Topographic surveying	
GPS	CMT-V, single-band, +/−1 m one std. deviation with post-acquisition, differential analysis; Garmin eTrex, +/−10 m in horizontal directions.
Total station theodolite	Sokkia SET 6 F (< +/− 5 cm in X and Z directions).
Processing software	Seismic Unix (Stockwell, 1999), seg2segy (Sioseis, 2011).
Processing flow for semblance velocity analysis	(1) Ormsby band-pass filtered with corner frequencies at 0, 3, 100, and 250 (Hz), (2) automatically gained (normalized by the RMS of an advance window of 0.1 s), (3) slope-filtered in f–k domain for noise, with reject slopes between −250, −175, −30, and 0 (samples/trace) and (4) semblance analysis.
Gray-scale seismic displays	Interpolated and re-balanced by division of RMS amplitude.

3. Field methods and data analysis

3.1. Seismic acquisition

Between September 2007 and February 2008, we collect cross-line-component (for horizontal shear- or S_H-wave) and vertical-component (for nominal compressional- or *P*-wave and vertical-shear or S_V waves) seismic data (Table 1, Figure 5). Because we conduct separate *P*-S_V and S_H experiments, we can distinguish when seismic arrivals are more probably direct-arrival shear waves rather than mode-converted shear waves (e.g., Figure 7, e.g., *P*-to-S_V), which might contaminate poorly placed geophones that are off-axis. In so doing we minimize the potential for deriving poor V_P–V_S ratios (Miller and Ivanov, 2005). Generally speaking, failure to separate the different body wave modes can lead to erroneous results (Park et al., 1998).

For the same frequency, slower S-waves may provide more resolution than *P*-waves in water-saturated, unconsolidated sediments (Stümpel et al., 1984; Harris, 2009). Love waves, S_H-reflected and S_H-refracted waves, can overlap and show similar apparent velocities in source-to-receiver-distance–traveltime (x–t) data plots and can be difficult to separate out (Miller et al., 2001). In this case, *P*-wave refraction data can provide a useful reference velocity-depth model, because Rayleigh wave phase velocities are usually distinctly lower than velocities for refracted P waves in the same setting.

At each of four areas along the levee, our field data acquisition geometry uses a fixed array of 24 geophones (horizontal- or vertical-component) with equally spaced seismic sources all in a straight line (Evans, 1997; Vincent et al., 2005), or pseudowalkaway geometry (Figure 6). The separation between sources equals the geophone array length and is chosen to provide laterally continuous, seismic returns while expediting data acquisition. In later analysis the data are rearranged as a function of the distance between the source and receiver locations under the assumption that along the line the geology is fairly homogeneous. Lateral subsurface heterogeneities can create small vertical time shifts (Figure 7), but these prove manageable for our data.

In order to determine whether seismic data can be used to detect changes in natural and artificial soils, both along and across the length of the levee axis, we chose four sites for seismic tests: three at the toe of the flood-protected, western levee flank (sites "N", "S" and A) and one on the flood-unprotected side, eastern levee flank (site A′). Two of these sites (Figure 5) lie 281 m (+/−30 m; site "N") north and 1104 m (+/−30 m; site "S") south, respectively, of the central sites where there is a visible surface crack. In order to examine possible 3-dimensional changes in subsurface geology, we also select a pseudowalkaway test site parallel to, and ~15 m (Figure 5) east of the levee crest at site A′. Sites A and A′ are located nearest where the crack width is greatest. These three sites on the flood-protected side are located ~30 m west of the levee crest so as to minimize the potentially strong flexural-mode effects along the levee crest (Miller and Ivanov, 2005) where the engineering fill is thickest. For each S_H test we generate two data sets of opposite polarities by hitting a small, embedded I-beam (Table 1) on opposite sides. Differencing the data sets attempts to double the amplitude of true S_H arrivals while attenuating converted *P*-wave modes (Helbig, 1986).

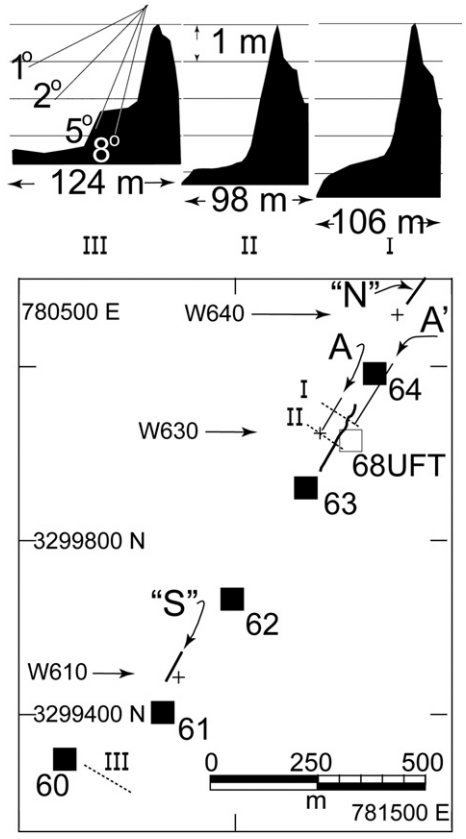

Fig. 5. Location of seismic experiments. Black lines denote largest extent of four seismic receiver–source arrays (sites "N", A, A (east and west of levee crest respectively) and "S"). Cone penetration test sites (solid-black boxes) follow axis of artificial levee crest (Figure 2). The wavy thin line marks location of crack, within a 2–3 m of the levee crest; accurate to +/− 1 m, 1 std. dev. Small crosses locate (+/− 10 m) local survey markers: W610, W630 (Figure 3) and W640, from south to north. Three topographic profiles (top) were taken on transects marked by small dotted lines (Roman numerals I–III) that run nearly at right angles to the levee crest. Profiles are shown with a vertical exaggeration of ~29 but relative surface-slope dips are indicated in degrees.

3.2. Seismic data analyses

Seismic data sets show P- and S-refracted as well as reflected arrivals (Figure 7). We attempt to map variations in the subsurface velocity field in order to detect changes in subsurface conditions (shear modulus) at four sites along the levee reach. We also evaluate the internal consistency of these perceived changes by cross-checking the velocity-vs.-depth estimates using two different methods. Forward modeling by ray tracing (Cerveny, 2001) best-matches the principal reflected and refracted seismic arrivals and obtains a simple, one-dimensional velocity-depth model that uses constant velocity and gradient velocity layers (Figures 8, 9). In order to highlight possible asymmetries in the subsurface between the eastern and western (protected) levee flanks adjacent to the cracks along the crest, we also construct contoured velocity profiles that differ only in that their central velocity-depth model comes from analysis of data taken either on the flood-protected side (site A) or flood-unprotected side (site A′). For each pair of contoured profiles, the velocity-depth models used at the northern and southern ends remain the same (Figures 9, 10).

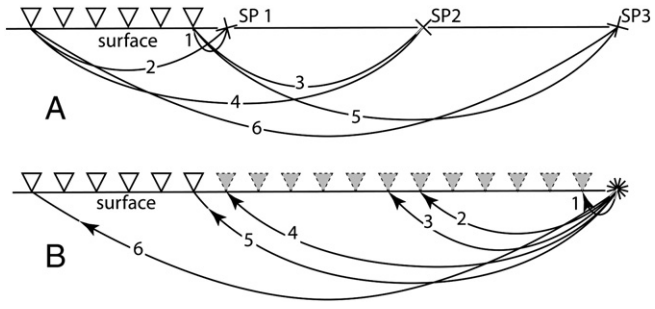

Fig. 6. Pseduowalkaway acquisition geometry. (A) Seismic data acquisition geometry in the field uses a pseudowalkaway layout which fixes geophones (solid triangles) but moves the source locations (three single crosses; SP 1–3). Two rays per source are shown. (B) Prior to velocity analysis, field data are rearranged as a function of the absolute distance between the seismic sources and the geophones (Figure 7). In this paper, the same geometry is scaled up to 24 geophones (Table 1).

Although our P-wave data sets lack clear, shallow seismic reflection arrivals, the S_H data sets do provide good reflections which we can use in a standard semblance-velocity analysis (Taner and Koehler, 1969; Stockwell, 1999) to analyze reflection arrivals (Figure 10). Shear wave data appear more sensitive to lithological contrasts that produce reflections (Stümpel et al., 1984). Reflection arrivals become apparent at later, two-way traveltimes (TWTT) (Figures 7) where they do not interfere with surface wave arrivals. Semblance velocity analysis performs a weighted correlation among traces in our pseudowalkaway gather to determine the best S_H move-out velocity. The resultant average velocity (Vrms)-depth models show velocity values which are averaged from the surface to the reflection arrival under consideration and should be lower than the corresponding 'local', refraction-derived velocities. For this analysis we isolate reflection arrivals by prior removal of all possible Love-wave arrivals in a standard processing flow (Table 1).

3.3. Topographic profiles and cone penetration test (CPT) Analyses

A comparison of three topographic cross-sections that cross the levee crest and seismic acquisition lines (Figures 2, 5) reveals significant differences in the shape of their flood-protected (W) flank slopes (max. ~8°). Crest-to-berm elevation difference can vary ~1–2 m along strike. In levee design plans (FFEB, 2007) the flood-protected, western slopes were projected to be almost identical in shape to each other, but since then, apparently, along-strike differences have appeared, which indicate that some differential subsidence may have occurred along this segment most notably in the central portion adjacent to the observed crest-line cracks.

Cone penetration testing (CPT) is a reliable method for distinguishing between sand and silt (Fellenius and Eslami, 2000), as in our shallow sediments (0–15 m) but may have more limited value in the presence of stiff clay (Chen, 2000), possibly at greater depths. CPT well sites are spaced every ~300 m (Figures 2, and 11) along the levee crest and toe (FFEB, 2007). Tip resistance (q_c) and sleeve friction (f_s) data are collected down to at least 20 m below the surface. From tables of q_c versus the friction ratio ($R_f = f_s/q_c$), in software we predict soil type/grain size (Mayne, 2007) or soil behavior types (SBT). For example, fine sands and silts are less cohesive than the organic-rich layers but have greater shear strength. As reference, we employ a commonly used interpretation chart (Robertson, 1990), which does not require pore-pressure data. The reference interpretation chart is modified in three ways. Because the behavior of the original eight (8) grain-size divisions in the clay-to-sand are similar, we simplify these ranges into clay, silt, and sand. Clay and organic material divisions are linearly extrapolated to higher values so as to include all calculated values of R_f. In order to differentiate between clay and peat, another division, organic clay, is added. The organic content of clay beneath the levee is of great significance, because it can reduce shear strength by increasing moisture retention and reducing density.

4. Results from seismic and CPT analyses

Forward, ray-trace-derived models of refracted and reflected seismic arrivals (V_S and V_P vs. depth) at all seismic sites show a common, noticeable increase in velocity at depths of 4–6 m (Figures 8, 9, 11, 12), either in the form of a discrete step (V_S) or high V_P gradient (~500 m/s in 5 m). These changes correspond to the top of a sand lobe (Figures 4, 12) seen

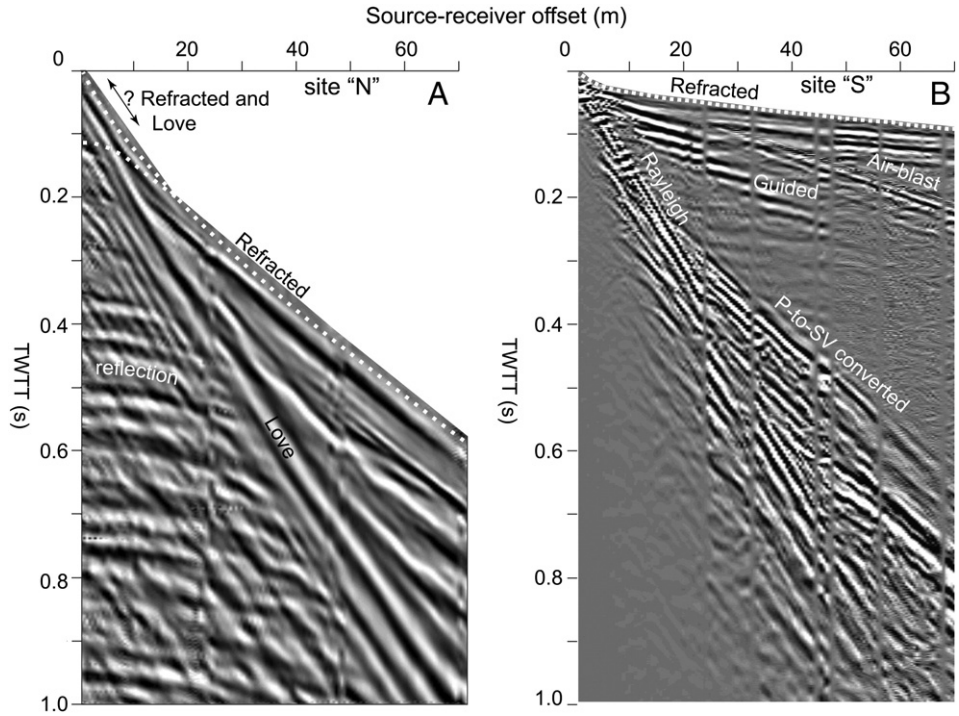

Fig. 7. Seismic data. (A) Pseudowalkaway shot gather from the northern site ("N") comprises 3 horizontal-component gathers with small static shifts every 24 m (geophone spacing = 1 m) caused by small lateral changes in velocity soil structure. Multiple S_H arrivals include guided or Love waves, refracted, and convex-shaped reflected arrivals, which are geometrically discordant with Love wave arrivals. Best-matched, ray-traced, time-based arrival picks (white dashes) are used to develop velocity-depth models (Figure 8). (B) Vertical-component, pseudowalkaway shot-gather data set from southern site ("S") with identical acquisition geometry. Intermediate velocity arrivals (~400 m/s) are interpreted as guided P/SV guided arrivals. Rayleigh wave arrivals show the lowest overall apparent velocity. Interpreted P-SV converted modes show velocity similar to S_H arrivals (A) and may emanate from the top of a shallow (5 m below levee flank depth) sand layer (Figure 3). Best-matched, ray-traced seismic arrivals are shown as white dashes.

in the interpreted CPT profile (Figure 11) at similar depths (+/−1 m), and that probably also corresponds to a sand unit from the former Saint Bernard delta (Frazier, 1967). Differences (+/−1 m) in the depth to the sand body may be the result of subsidence since the CPT data were collected.

Depths are similar to the top of the interpreted sand unit among the different seismic models (Figure 8). However, overall V_S values show their greatest overall change across the damaged crest, between sites A (protected) and A′ (unprotected). The smallest overall V_S values are found on the protected side of the levee. Barring unrealistic changes in bulk density, lower values for V_S at site A may indicate a lower shear modulus (low-strain) on the protected side. In contrast, and in the 0–10 m depth range, corresponding V_P-depth profiles are relatively higher on the same side and may indicate a greater saturation for similar depths than under site A′ (unprotected). V_S-depth profiles derived by semblance analysis (V_{RMS}; Figure 10) also show that overall, these values are lower at site A (protected side) than at site A′ (unprotected side), in the deeper subsurface (>4 m and >0.3 s TWTT).

Vp–Vs ratios provide a convenient single value, useful for detecting unusual changes in elastic material properties (Dunbar et al., 2007). Larger V_P/V_S values help highlight the greater increase of V_P with depth than V_S with depth. From contoured velocity profiles (Figure 9) at relatively shallow depths of 3–5 m, V_P–V_S ratios appear relatively high (8 or 9) at site A (protected side), whereas these ratios are only 4–5 at equivalent depths at site A′ (unprotected side).

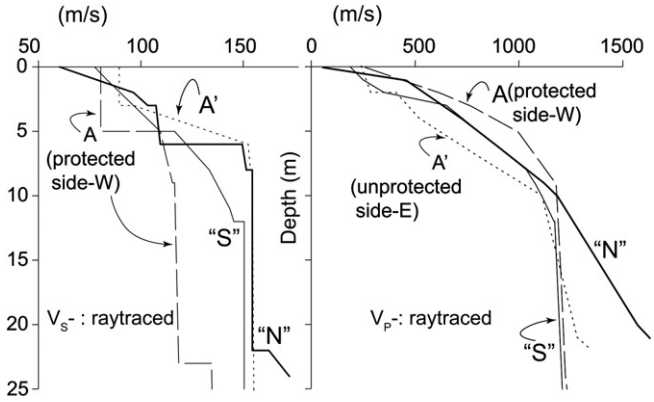

Fig. 8. Ray-traced velocity-depth models. An overplot of all velocity-depth models for *P* and S_H waves derived from forward ray tracing of seismic pseudowalkaway seismic profiles (e.g., Figure 7). Models are derived for data from the flood-protected levee flank at the northernmost ("N") and southernmost ("S") sites; sites A and A′ lie respectively on the flood-protected and unprotected flanks in the vicinity of crestal cracks (Figures 3, 5, 11). Depths are referenced to protected toe-of-levee elevation.

5. Discussion

In our study area subsurface, fluvial–deltaic sediments (Saucier and Snowden, 1995) and their geotechnical properties may vary, laterally (Allen and Allen, 2005). Seismic acquisition tools are a cheaper complementary tool which may be used to locate anomalous zones and help target additional geotechnical sites. As an example of the value of this approach, we examine a crack along the crest of a levee that is located, coincidentally, between available CPT-geotechnical sites (Figure 2). In the interpreted CPT-profile, nearby soil types and their distribution (Figure 11) are similar to those found elsewhere where no cracks appear. Although our seismic sites do not provide a continuous sampling of the sub-levee materials, velocity-depth trends are consistent between S_H and *P*-wave data sets, two types of velocity analyses and with a major clay–sand boundary interpreted in a CPT-profile. Interpretations of the seismic velocity analyses suggest that the largest physical property anomalies occur across the distressed levee area and should therefore be a future site of interest for additional geotechnical investigations.

In this sedimentary environment better reflector arrivals appear in the S_H than in the *P*-wave data (Figure 7), so that laterally continuous S_H reflection profiles should be obtainable in the future. Continuous

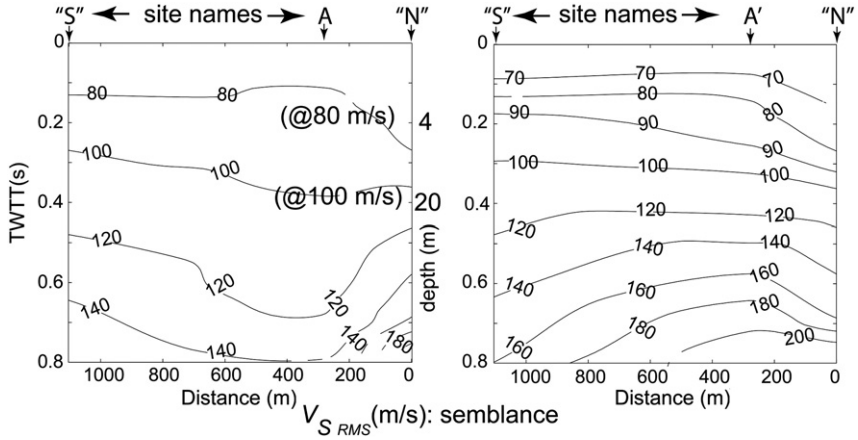

Fig. 9. Contour plot of V_P–V_S ratios (Figure 8). Velocity-depth contours (via cubic-spline interpolation) are constructed using only three 1-D velocity-depth (V–z) profiles (maximum source–receiver offset ranges of 72 to 168 m), centered at locations marked using vertical arrow heads. Cross-sections on left use V–z models from experiments on the flood-protected west side of the levee. Cross-sections on the right share the same V–z model along their edges but are different because they have a central V–z model collected on the flood-unprotected side. The results of the site taken higher on the unprotected levee flank are adjusted by the ~2-m +/− .2 height difference above the other three sites on the protected side. Depths are referenced to protected toe-of-levee elevation.

profiles can correlate V_S values against CPT values where the seismic lines cross the geotechnical site (Hegazy and Mayne, 1995; Stuedlein, 2010). These empirical correlations improve if the sediment type is also identifiable. We can use the CPT data from a geotechnical boring site near the crack along the crest to compare CPT-derived V_S and seismically-derived V_S values (Figure 12) created using the following empirical statistical relations from Hegazy and Mayne (1995).

$$V_s = 12.02 q_c^{0.319} f_s^{-0.0466}, \quad (1)$$

predicts higher V_S values in sand and hence better explains the seismically-derived V_S values at depths below approximately 5-6 m whereas

$$V_s = (10.1\ Log\ q_c - 11.4)^{1.67} \left(\frac{f_s}{q_c} * 100\right)^{0.3}, \quad (2)$$

which is derived for mixtures of clay and sand soils, is more appropriate for matching the shallower V_S values of the site. There is additional potential to derive shear strength from degradation curves (Davich et al., 2004), cross-plots of the in-lab and field seismic data values (Na et al., 2005), or through intermediate CPT strength and seismic velocity relations. Interpolation between known geotechnical well sites can also be achieved by common, geostatistical, deterministic methods like kriging, although these lead to the development of smooth property variations which are often not representative of the complex nature of fluvial–deltaic geology. Other techniques that are stochastic-process or random-process based may allow more variability (Kalla, 2008) but can improve by integrating seismic properties.

The cone penetration test is most accurate when the measured tip resistance (q_c — kPa) is corrected for pore pressure and overburden. Positive pore pressure reduces the normal stress lower tip resistance and effectively weakens the sediment. Corrections can reveal silt that appeared to be sand, clay that appeared to be silt, and organic material that appeared to be clay. Negative pore pressures, especially in sandier soils (e.g., Elsworth et al., 2006) can have the opposite effect. Although we do not have access to pore-pressure measurements, our results would not change substantially. Our interpretation of the major appearance of sand agrees with geological estimates and other physical property results (Figure 4) and since shallow levee building material (0–~3 m) is ideally clay-rich, we did not expect it to deviate toward coarser grain sizes. CPT interpretations using the standard Robertson (1990) chart indicate a high concentration of organic-rich materials within the earthen levee but not particularly concentrated under the zone that shows cracks along the crest.

We can use theoretical considerations to interpret possible water saturation changes between site A (protected side) and site A′ (unprotected side). If we assume that the natural sediment types are similar between closely-spaced sites, then the larger V_P values on the protected

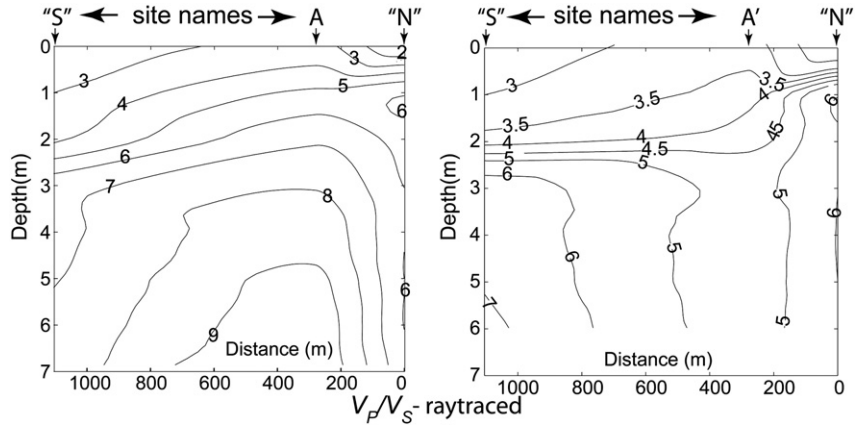

Fig. 10. Semblance-derived velocity-depth models. Contours (100 m/s interval) of V_S values (V_{rms}). Depths are referenced to protected toe-of-levee elevation. See Fig. 9 for additional construction details.

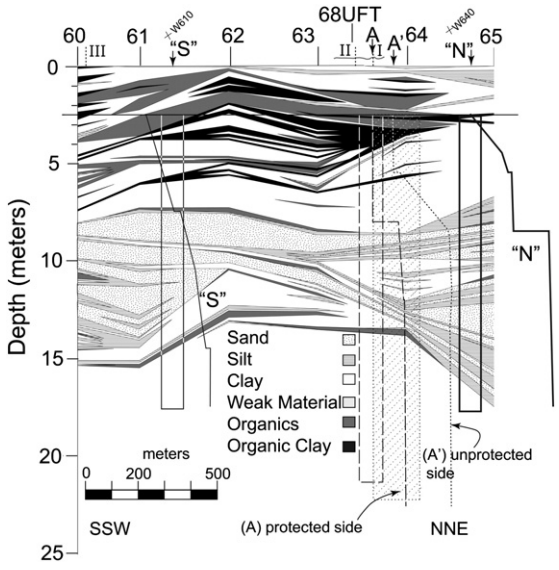

Fig. 11. Integrated CPT and seismic results. Cone-penetrometer test (FFEB, 2007) data-derived cross-section, showing six different interpreted soil behavior types. Four areas enclosed by rectangles show the lateral extent of subsurface sampled by pseudowalkaway profiles projected on to the line, from up to 30 m away, from the east (site A′) or west (sites "S", A, "N"). The largest enclosed rectangle corresponds to the pseudowalkaway profile taken on the flood-unprotected side of the levee crest (east). Reference toe-of-levee lies ~2.5 m below the crest. Tests along the center of the artificial levee crest are located at regular intervals, referenced by numbers. Samples for laboratory testing (Figure 4) are taken at well (68UFT), marked with a continuous vertical line. V_S-depth models (Figure 8) are superimposed. Several features shown in Fig. 2 are cross-referenced along the top axis, such as (1) the map shape of the levee crack. (2) Vertical dashed lines locate where topographic profiles cross the levee axis. (3) Crosses locate local levee survey markers (W 610—southernmost, W640—northernmost) along the protected levee flank. (4) Roman numerals locate levee topographic profiles (Figure 5). Depths are referenced to crest of levee elevation, but long horizontal line marks the toe-of-levee elevation.

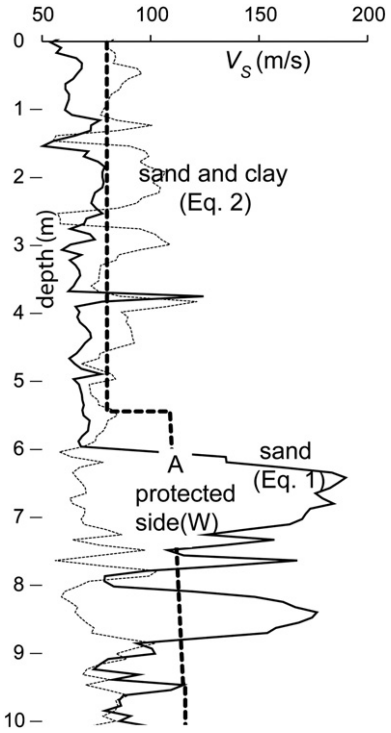

Fig. 12. Applied statistical correlation equations. Two common empirical relations between V_S and CPT data (Hegazy and Mayne, 1995) are applied to tip resistance and sleeve friction values from CPT site 63 (Figures 2, 5, 11). One relation is derived for mixtures of clay and sand (smallest dashes) and another for dominantly, sand (continuous line).

side for the same depth indicate a greater degree of saturation. Effective medium theory can be used to predict seismic velocities (Bachrach and Nur, 1998) in sand-rich sediments, as well as in clay-rich shales (Avseth et al., 2005). We expect that for granular soils, only where near-full saturation is approached (>99%), does V_P increase to order 10^3 m/s. At conditions just below full saturation (<99%) V_P can be much smaller, of order 10^2 m/s. If saturation is greater on the protected side then full saturation is probably not achieved until depths of 5–10 m, coincident with reworked delta sand (Figures 2, 11). Perhaps because of the lesser organic content in the sand there is also a decrease in the amount of any in-situ biogenic gas. Even in marine settings, where high-porosity sediments (~60%) are nominally saturated, small amounts of gas (~1% of overall porosity) can keep V_P in the same low range (Anderson and Hampton, 1980). Shear waves are assumed to remain relatively unaffected (Domenico and Danbom, 1986) by pore fluid composition in partially saturated- to fully saturated soils, except by way of the increased overall density, which can slightly reduce measured velocities (Velea et al., 2000).

V_P–V_S ratios can help highlight the transition to areas where saturation is complete. High (5–6) values of V_P/V_S (dynamic Poisson's ratio slightly less than 0.5) derived from seismic data (Figure 9) are not unusual in shallow unconsolidated sediments. Similar values have been detected in soft sediments from both field seismic experiments (Jongmans et al., 1996) and laboratory seismic experiments (Zimmer et al., 2002), and are also a useful indicator of proximity to the water table (Liu et al., 1997; Guy, 2006). For our types of sedimentary environments that comprise shallow (0–15 m) organic-rich soils, *Vs* values are naturally extremely low (Campanella et al., 1994), and increase the V_P–V_S ratio further. The lower V_S values at site A (protected side) than at A′ (unprotected side) are such a case. Commonly, in earthquake site characterization studies, spectral ratios of the seismic horizontal and vertical ground motion (e.g., Nakamura, 1989) are used to detect the resonance thickness of shallow soft layers. This empirical technique is sensitive to large V_S velocity contrasts with depth (Figure 8) assuming that V_P/V_S does not change. In cases where V_P/V_S does change with depth crustal studies show that a joint inversion (Lin et al., 2012) of the Rayleigh surface wave dispersion curves and horizontal/vertical ratios remains promising.

Differential surface subsidence (Figure 5) may reflect a heterogeneous distribution of sub-levee materials along, and could be a likely cause for observed levee cracks (Figure 13). We can reasonably assume that these changes occur over distances smaller than the spacing between geotechnical sites (~300 m) but of comparable size to the crack length (~100 m), and in all directions, although our interpretations concentrate on changes along the length of the levee flanks. Marked differences in V_P values between sites A (protected side) and A′ (unprotected side) over even smaller distances of 30–40 m may be the result of marked changes in the sediment types. However, at present, surface sediment type distribution maps (Figures 1, 2) and the interpreted CPT-profile (Figure 11) support larger scale changes and this interpretation appears less valid. In future, parallel, continuous, seismic profiles on either side of the levee crest may be needed to examine the significant changes over distances as small as the levee width itself, <~100 m.

Although the influence of soil shrinkage by desiccation is not completely excluded, the more curved map-view shape along the northern half of the levee cracks suggests at least possible slumping down-to-the-west. Simple models (Fredlund and Rahardjo, 1993; Eqs. 11–12) suggest that wider desiccation cracks could indicate substantially deeper water table toward the northern range of the crack. At present we have not verified this prediction directly but we note the much shallower depth to higher V_P values on the western protected levee side that would imply the opposite: a shallower water table depth. From October 2007 through February 2008, the period of time during which seismic data were collected, no significant changes appeared in the size and shape of the cracks, which presumably remained stable over this time.

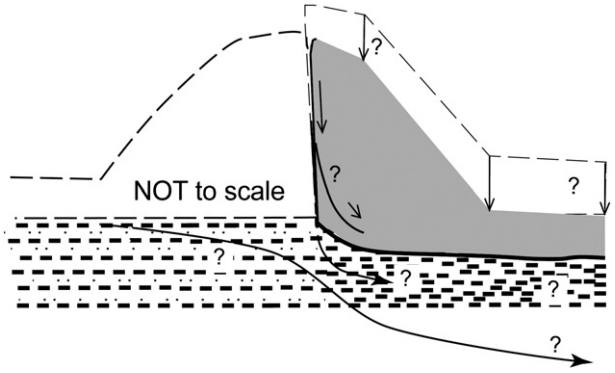

Fig. 13. Conceptual interpretation distressed levee (not to scale). Compaction, primarily in underlying organic-rich soils on the protected side, creates surface subsidence and accompanying cracks. Arrows hypothesize hydrological flow paths. Only the right side of the schematic cross-section is surveyed (Figure 5).

In the fresh-water swamp and marsh sedimentary environments of our study area, we expect that materials with the least cohesive strength and lowest shear strength (Figure 4) and V_S values (Figure 8) will correspond to sediments that are more organic-rich, less consolidated. Point bar and levee deposits consist of fine sands and silts and represent the stronger end of the spectrum. Sands can liquefy and the organic-rich silts can act as a good lubricant with very little or no residual strength after movement is initiated (Rogers et al., 2008).

If some degree of slope failure were responsible for the curvilinear cracks along the crest, we did not note a topographic toe-of-slope bulge or other cracks to the west that could be associated with displacement of sediment at depth. These predicted disruptions are absent either because slope displacement is insignificant, or surface damage lies farther to the west and outside the surveyed area within the levee-fill borrow pit (Figure 2). In all cases, slight topographic changes on the levee slope may be overwhelmed by differential settling effects (Figure 5). Any hidden degree of slope failure can remold soils, reduce their shear strength (Rogers et al., 2008) and act to increase permeability (Figure 13). If sediments have undergone some deformation then we may expect lower V_S values as observed at site A (protected side) adjacent to the cracks along the crest. Local faults (Figure 1) mapped below surface (Wallace, 1957) are not suitable candidates to induce levee damage because they are either too distant and at too high an angle to the orientation of levee cracks to be likely causes of the observed cracks. More recent maps of surface faults in nearby New Orleans (Dokka, 2011) indicate that vertical motion is more readily interpreted as the indirect result of local subsurface water extraction.

6. Conclusions

Traditional geotechnical estimates of sub-levee soils may be enhanced by seismic field sampling between sites. Even where subsurface geotechnical data exist, they are, normally, only collected at widely spaced intervals, often >60–100 m apart, unable to detect variable sedimentary types. In the field study area, south of New Orleans, seismic velocity-versus depth models increase markedly across a sediment change between organic-rich and sand units, based on interpreted cone penetration testing data. Also, the largest V_P–V_S ratios (8–9) occur near this depth. V_P values remain low (order 10^2 m/s) above this depth (despite being 5 m below sea-level) because of the possible presence of small amounts of gas in the organic-rich sediments. The surface seismic data sets reconfirm that in the organic-rich sedimentary environment of the study area only S_H seismic data displays reflection arrivals although useful refractions in both the P and S_H data. In addition to velocity-versus-depth models derived from the refracted arrivals, V_S reflector arrivals lend themselves to traditional velocity semblance analysis and can be used to reconfirm refraction-derived models.

Several possible causes for the appearance of cracks along the levee crest may be related to unexpected organic-rich materials used during the construction and large lateral changes in subsurface materials that may lead to variable differential compaction.

Future preventive monitoring of flood-protection barriers stands to benefit from integration of existing civil engineering, geological and topographic information correlated to data from geophysical profiles, which can then be used to extrapolate between sites and locate anomalies in physical properties although multiple non-invasive geophysical electrical methods which are sensitive to fluids should also be considered.

Acknowledgments

Hicks completed his M.Sc. supported by a National Science Foundation grant (GEO-0303138). Field student support was provided generously to Lorenzo by the Southeast Louisiana Flood Protection Authority-East and West, American Petroleum Institute Delta Chapter, New Orleans Geological Society and Southeastern Geophysical Society of New Orleans. We are very grateful to M. Merritt who introduced us to levees and to G. Spohrer, for their continuous support and encouragement and to our student field assistants: M. Al Tammar, A. Wahbi, W. Blake and V. Adams. This manuscript improved immensely thanks to the very thorough and constructive reviews of two anonymous reviewers.

References

Akpokodje, E.G., 1989. Preliminary studies on the geotechnical characteristics of the Niger delta subsoils. Eng. Geol. 26, 247–259.
Allen, P., Allen, J., 2005. Basin Analysis: Principles and Applications, 2nd ed. Blackwell.
Andersen, C.F., Battjes, J.A., Daniel, D., Edge, B., Espey, W., Gilbert, R.B., Jackson, T.L., Kennedy, D., Mileti, D.S., Mitchell, J.K., Nicholson, P., Pugh, C.A., Tamaro Jr., G., Traver, R., 2007. The New Orleans Hurricane Protection System: What Went Wrong and Why: A Report by the Amer. Soc. Civil Engin., Hurricane Katrina External Review Panel. Amer. Soc. Civil Engin., Reston, VA.
Anderson, A.L., Hampton, L.D., 1980. Acoustics of Gas-bearing Sediments. II. Measurements and Models. J. Acoust. Soc. Am. 67, 1890–1903.
Avseth, P., Mukerji, T., Mavko, G., 2005. Quantitative Seismic Interpretation: Applying Rock Physics Tools to Reduce Interpretation Risk. Cambridge Univ. Press.
Bachrach, R., Nur, A., 1998. High-resolution Shallow-seismic Experiments in Sand, Part I: Water Table, Fluid Flow, and Saturation. Geophysics 63, 1225–1233.
Blum, M.D., Roberts, H.H., 2009. Drowning of the Mississippi Delta due to insufficient sediment supply and global sea-level rise. Nat. Geosci. 2, 488–491.
Boutwell, G.P., 2007. Geotechnical Engineering Difficulties and Soil Conditions in Southeast Louisiana, Embankments, Dams, and Slopes (GSP 161), 40905 ed. ASCE, Denver, Colorado, USA 15.
Bromhead, E.N., 1986. The Stability of Slopes. Surrey Univ. Press.
Campanella, R.G., Stewart, W.P., Roy, D., Davies, P., 1994. Low strain dynamic characteristics of soils with the downhole pieozocone penetrometer. In: Ebelhar, R.J., Drnevich, V.P., Kutter, B.L. (Eds.), Dynamic Geotechnical Testing II. Amer. Soc. Testing Materials.
Cerveny, V., 2001. Seismic Ray Theory. Cambridge Univ. Press.
Chen, F.H., 2000. Soil Engineering: Testing, Design, and Remediation. CRC Press.
Cobos-Roa, D., Bea, R.G., 2008. Three-dimensional seepage effects at three New Orleans levee breaches during hurricane Katrina. Electron. J. Geotech. Eng. 13.
Davich, P., Labuz, J., Guzina, B., Drescher, A., 2004. Small strain and resilient modulus testing of granular soils. Transport. Res. Record. Cent. Transport. Stud.Univ. of Minnesota.
Dokka, R.K., 2011. The role of deep processes in late 20th century subsidence of New Orleans and coastal areas of southern Louisiana and Mississippi. J. Geophys. Res. 116, B06403.
Domenico, S.N., Danbom, S.H., 1986. Shear-wave technology in petroleum exploration — past, current, and future. In: Danbom, S.H., Domenico, S.N. (Eds.), Shear-Wave Explor. Geophys. Develop. Series. Soc. Explor. Geophys., Tulsa, pp. 3–18.
Dunbar, J.B., Britsch III, L.D., 2008. Geology of the New Orleans Area and the canal levee failures. J. Geotech. Geoenviron. Eng. 134, 566–582.
Dunbar, J.B., Torrey III, V.H., Wakeley, L.D., 1999. A Case History of Embankment Failure: Geological and Geotech. Aspects of the Celotex Levee Failure, New Orleans, Louisiana. U.S. Army Corps Engin., Engin. Res. Develop. Cent.
Dunbar, J.B., Llopis, J.L., Sills, G.L., Smith, E.W., Miller, R.D., Ivanov, J., Corwin, R.F., 2007. Condition Assessment of Levees, U.S. Section of the International Boundary and Water Commission: Flood Simulation Study of Retamal Levee, Lower Rio Grande Valley, Texas, Using Seismic and Electrical Geophysical Models. US Army Corps Engin., Engin. Res. Develop. Cent.
Dyer, M.R., 2005. Further tests on the fissuring of clay fill at the thorngumbald flood embankment. In: Tarantino, A., Romero, E.J., Cui, Y.J. (Eds.), Advanced Experimental Unsaturated Soil Mechanics. Taylor and Francis, London, Trento, Italy, pp. 501–504.
Elsworth, D., Lee, D.S., Hryciw, R., Shin, S., 2006. Pore pressure response following undrained uCPT sounding in a dilating soil. J. Geotech. Geoenviron. Eng. 132/11, 1485–1495.
Evans, B.J., 1997. A Handbook for Seismic data Acquisition in Exploration. Soc. Explor. Geophys., Tulsa.

Fellenius, B.H., Eslami, A., 2000. Soil Profile Interpreted from CPTu Data Geotech. Engin. Conference.
FFEB, 2007. Joint Venture, Geotech. Consultants. Task Order 0008 Geotechnical Design Report V-line Levee (East of Vertex) and Harvey Canal Levee.Dept. Army, New Orleans District, Corps Eng., New Orleans, Louisiana (29 pp.).
Frazier, D.E., 1967. Recent deltaic deposits of the Mississippi River: their development and chronology. Gulf Coast Assoc. Geol. Soc. 17, 287–315.
Fredlund, D.G., Rahardjo, H., 1993. Soil Mechanics for Unsaturated Soils. Wiley, NY.
Gagliano, S.M., van Beek, J.L., 1970. Geological and geomorphic aspects of deltaic processes, Mississippi delta system. Hydrol. Geol. Studies Coast. Louisiana, Rept. 1, Coast. Resources Prog. Cent. Wetland Resources.Louisiana State Univ., Baton Rouge.
Galloway, D., Jones, D.R., Ingebritsen, S.E., 1999. Land subsidence in the United States. US Department of the Interior, Circular 1182.U.S. Geol. Surv., Reston, VA.
U.S. Geol. Surv., 1947. Bertrandville Quadrangle, 1:62,500, Topographic Map, Washington, D.C.
Grelle, G., Guadagno, F.M., 2009. Seismic refraction methodology for groundwater level determination: "water seismic index". J. Appl. Geophys. 68, 301–320.
Guy, E.D., 2006. High-resolution P- and S-wave seismic reflection investigation of a shallow stratigraphic sequence. Electron. J. Geotech. Eng. 11/B.
Hammah, R.E., Curran, J.H., 2006. Geostatistics in geotechechnical engineering: fad or empowering? GeoCongress 1–5 (2006).
Harris, J., 2009. Hammer-impact SH-wave seismic reflection methods in neotectonic investigations: general observations and case histories from the Mississippi Embayment, U.S.A. J. Earth Sci. 20, 513–525.
Hegazy, Y.A., Mayne, P.W., 1995. Statistical correlations between Vs and cone penetration data for different soil types. Internat. symp. on cone penetration testing. Swedish Geotech. Soc, Linkoping, Sweden.
Helbig, K., 1986. Shear waves — what they are and how they can be used. In: Danbom, S.H., Domenico, S.N. (Eds.), Shear-Wave Explor. Geophys. Develop. Series. Soc. of Explor. Geophys., Tulsa, pp. 19–36.
Inazaki, T., Tadahiko, S., 2005. Geotechnical Characterization of Levee by Integrated Geophysical Surveying. Public Works Res. Inst., Japan.
Jongmans, D., Demanet, D., Horrent, C., Campillo, M., Sanchez-Sesma, F.J., 1996. Dynamic soil parameters determination by geophysical prospecting in Mexico City: implication for site effect modeling. Soil Dyn. Earthq. Eng. 15, 549–559.
Julien, P.Y., 2002. River Mechanics. Cambridge Univ. Press.
Kalla, S., 2008. Reservoir characterization using seismic inversion data, Petrol. Engin. Louisiana State Univ., Baton Rouge (150 pp.).
Karl, L., Fechner, T., Schevenels, M., François, S., Degrande, G., 2011. Geotechnical characterization of a river dyke by surface waves. Near Surf. Geophys. 9, 515–527.
Kolb, C.R., Van Lopik, J.R., 1958. Geology of the Mississippi River deltaic plain, southeastern Louisiana. U.S. Army Engin. Waterways Experiment Station, Vicksburg, MS.
Lane Jr., J.W., Ivanov, J., Day-Lewis, F.D., Clemens, D., Patev, R., Miller, R.D., 2008. Levee evaluation using MASW: preliminary findings from the Citrus Lakefront levee, New Orleans, Louisiana. Symp. Appl. Geophys. to Engin. Environ. Problems, 21, pp. 703–712.
Lee Jr., L.T., Wibowo, J.L., Taylor, P.A., Glynn, M.E., 2009. In situ erosion testing and clay levee erodibility. J. Environ. Eng. Geosci. 15, 101–106.
Lin, F.-C., Schmandt, B., Tsai, V.C., 2012. Joint inversion of Rayleigh wave phase velocity and ellipticity using USArray: constraining velocity and density structure in the upper crust. 39/12, L12303. http://dx.doi.org/10.1029/2012GL052196.
Link, L.E., Jaeger, J.J., 2009. Performance evaluation of the New Orleans and southeast Louisiana hurricane protection system. Final Report of the Interagency Performance Evaluation Task Force. U.S. Army Corps Engin (https://ipet.wes.army.mil).
Liu, H.-P., Hu, Y., Dorman, J., Chang, T.-S., Chiu, J.-M., 1997. Upper Mississippi embayment shallow seismic velocities measured in situ. Eng. Geol. 46, 313–330.
Mayne, P.W., 2007. Cone penetration testing. NCHRP Synthesis of Highway Practice 368. Transport. Res. Board, NRC, Washington, D.C.(117 pp.).
McFarlan Jr., E., 1961. Radiocarbon Dating of Late Quaternary Deposits, South Louisiana, 72. Geol. Soc. Amer. Bull., Boulder, CO, U.S., pp. 129–158.
Mesri, G., Ajlouni, M., 2007. Engineering properties of fibrous peats. J. Geotech. Geoenviron. Eng. 133, 850–866.
Miall, A.D., 2000. Principles of Basin Sedimentary Analysis, 3rd ed. Springer.
Miller, R.D., Ivanov, J., 2005. Seismic Tests on IBWC Levees: Weslaco, Texas, Open-file Report. U.S. Army Corps Engin.
Miller, R.D., Xia, J., Park, C.B., 2001. Love Waves: A Menace to Shallow Shear Wave Reflection Surveying.
Na, Y.-M., Choa, V., Teh, C.-I., Chang, M.-f, 2005. Geotechnical Parameters of Reclaimed Sandfill from the Cone Penetration Test. NRC, Canada.
Nakamura, Y., 1989. A method for dynamic characteristic estimation of subsurface using microtremor on the ground surface. Q. Rep. Railway Tech. Res. Inst., 30 25–33.
National Oceanic and Oceanographic Admin. (U.S.), 2011. Comparative Climatic Data for the United States Through 2011. U.S. Gov. 4 (www1.ncdc.noaa.gov/pub/data/ccd-data/CCD-2011.pdf).
U.S. Navy, 1952. 1:40,000 MDA Aerial Photogaph in: Louisiana State Univ. Cartograph. Inform. Cent. Frame 45-9 Flight Line V2 Patrol VP-61 Date 2-5-1952 Time 20:40.
Neill, J.D., 1990. Use of Electromagnetic Methods for Groundwater Studies. In: Ward, S.H. (Ed.), Geotechnical and Environmental Geophysics, Soc. Explor. Geophys., Tulsa, OK, pp. 191–218.
Niederleithinger, E., Weller, A., Lewis, R., 2012. Evaluation of geophysical techniques for dike inspection. J. Environ. Eng. Geophys. 17, 185–195.
Nyman, J.A., Delaune, R.D., Patrick, W.H., 1990. Wetland soil formation in the rapidly subsiding Mississippi River deltaic plain: mineral and organic matter relationships. Estuar. Coast. Shelf Sci. 31, 57–69.
Park, C.B., Miller, R.D., Xia, J., 1998. Imaging dispersion curves of surface waves on multi-channel record. 68th Annual Intern. Meet. Soc. Explor. Geophys. Expand. Abstr, pp. 1377–1380.
Peltier, W.R., Fairbanks, R.G., 2006. Global glacial ice volume and Last Glacial Maximum duration from an extended Barbados sea level record. Quat. Sci. Rev. 25, 3322–3337.
Reading, H.G., 1998. Sedimentary Environments: Processes, Facies, and Stratigraphy, 3rd ed. Blackwell Sci., London.
Robertson, P.K., 1990. Soil classification using the cone penetration test. Can. Geotech. J. 27, 151–158.
Rogers, J.D., Boutwell, G.P., Schmitz, D.W., Karadeniz, D., Watkins, C.M., Athanasopoulos-Zekkos, A.G., Cobos-Roa, D., 2008. Geologic conditions underlying the 2005 17th Street Canal levee failure in New Orleans. J. Geotech. Geoenviron. Eng. 134, 583–601.
Santamarina, J.C., Rinaldi, V.A., Fratta, D., Klein, K.A., Wang, Y.-H., Cho, G.C., Cascante, G., 2005. A survey of elastic and electromagnetic properties of near-surface coils. In: Butler, D.K. (Ed.), Near-surface Geophysics, Soc. of Explor. Geophys., Tulsa, OK, pp. 71–88.
Saucier, R.T., 1994. Geomorphology and Quaternary Geologic History of the Lower Mississippi Valley. US Army Corps Engin. Waterways Experiment Station, Vicksburg, MS.
Saucier, R., Snowden, J., 1995. Engin. geology of the New Orleans area. Field Trip Guide Book #6a &6b. Geol. Soc. Amer., pp. 131–153.
Seed, R.B., Bea, R.G., Abdelmalak, R.I., Athanasopoulos, A.G., Boutwell, G.P., Bray, J.D., Briaud, J.-L., Cheung, C., Cobos-Roa, D., Cohen-Waeber, J., Collins, B.D., Ehrensing, L., Farber, D., Hanemann, M., Harder, L.F., Inkabi, K.S., Kammerer, A.M., Karadeniz, D., Kayen, R.E., Moss, R.E.S., Nicks, J., Nimmala, S., Pestana, J.M., Porter, J., Rhee, K., Riemer, M.F., Roberts, K., Rogers, J.D., Storesund, R., Govindasamy, A.V., Vera-Grunauer, X., Wartman, J.E., Watkins, C.M., Wenk Jr., E., Yim, S.C., 2006. Investigation of the Performance of the New Orleans Flood Protection System in Hurricane Katrina on August 29, 2005.
Sioseis, 2011. A computer System for Enhancing and Manipulating Marine Seismic Reflection and Refraction Data. (Accessed Aug. 1, sioseis.ucsd.edu/sioseis.html).
Stockwell, J.W., 1999. The CWP/SU: Seismic Unix package. Comput. Geosci. 25, 415–419.
Stuedlein, A., 2010. Shear-wave velocity correlations for Puyallup River alluvium. J. Geotech. Geoenviron. Eng. 136, 1298–1304.
Stümpel, H., Kähler, S., Meissner, R., Milkereit, B., 1984. The use of seismic shear waves and compressional waves for lithological problems of shallow sediments. Geophys. Prospect. 32, 662–675.
Taner, M.T., Koehler, F., 1969. Velocity spectra—digital computer derivation applications of velocity functions. Geophysics 34, 859–881.
Tornqvist, T.E., Gonzalez, J.L., Newsom, L.A., van der Borg, K., de Jong, A.F.M., Kurnik, C.W., 2004. Deciphering Holocene sea-level history on the U.S. Gulf Coast; a high-resolution record from the Mississippi Delta. Geol. Soc. Am. Bull. 116, 1026–1039.
Turnbull, W.J., Krinitzsky, E.L., Weaver, F.J., 1966. Erosion in Soils of the Lower Mississippi Valley, J. of the Soil Mechanics and Foundation Division. Proc. Am. Soc. Civ. Eng. 121–136.
Turner, E.R., 2004. Coastal wetland subsidence arising from local hydrologic manipulations. Estuar. Coasts 27, 265–272.
Ulusay, R., Tuncay, E., Hasancebi, N., 2010. Geo-engineering properties and settlement of peaty soils at an industrial site (Turkey). Bull. Eng. Geol. Environ. 69, 397–410.
USACE, 2003. Digital Elevation Model (USGS DEM), Bertrandville Quadrangle, Louisiana, UTM 15 NAD83, Louisiana, Contract Number DACW43-00D-0511 0014, Task Order 05, Saint Louis District.
Velea, D., Shields, F.D., Sabatier, J.M., 2000. Elastic wave velocities in partially saturated Ottawa Sand: experimental results and modeling. Soil Sci. Soc. Am. J. 64, 1226–1234.
Vincent, P.D., Steeples, D.W., Tsoflias, G.P., Sloan, S.D., 2005. Two approaches to noise tests. Soc. Explor. Geophys. Tech. Prog. Expand. Abstr. 24, 1180–1183.
Wallace, W.E., 1957. Fault map of South Louisiana. Trans. Gulf Coast Assoc. Geol. Soc. 7, 240–241.
Wehling, T.M., Boulanger, R.W., Arulnathan, R., Harder, J.L.F., Driller, M.W., 2003. Nonlinear dynamic properties of a fibrous organic soil. J. Geotech. Geoenviron. Eng. 129, 929–939.
Zhody, A.A.R., Eaton, G.P., Mabey, D.R., 1974. Application of Surface Geophysics to Ground-water Investigations: Techniques of Water-resources Investigations of the U.S. Geol. Surv (116 pp.).
Zimmer, M., Prasad, M., Mavko, G., 2002. Pressure and porosity influences on V_P–V_S ratio in unconsolidated sands. Lead. Edge 21, 178–183.